Title: Ciliary ARLs drive renal cystogenesis

Robert E. Van Sciver[1,2], Avery Forster[3] and Tamara Caspary[1,‡]

[1]Department of Human Genetics, Emory University School of Medicine, 615 Michael Street, Suite 301, Atlanta, GA 30322, USA
[2]Current address: Department of Cell, Developmental, and Integrative Biology, University of Alabama at Birmingham Heersink School of Medicine, 1918 University Boulevard, McCallum 227, Birmingham, AL 35233, USA
[3]Dana-Farber Cancer Institute, 375 Longwood Ave, LW-745, Boston, MA 02115

[‡]Address correspondence to: Tamara Caspary (tcaspar@emory.edu), 404-727-9862

ORCID and email for authors:
Robert E. Van Sciver, 0000-0002-1818-2661, rvansciv@uab.edu
Avery Forster, 0009-0003-3037-2059, aforster@bu.edu
Tamara Caspary, 0000-0002-6579-7589, tcaspar@emory.edu

Keywords: polycystic kidney disease, cilia, ARL GTPases, polycystins

Abstract word count: 274

Text word count: 4394

Number of figures and tables: 6 figures; no tables

Key Points

- Loss of ciliary ARL13B or mutating the residue critical for its GEF activity do not affect renal morphology or physiology in adult mouse models
- Loss of ciliary ARL13B suppresses renal cystogenesis in an adult mouse model of polycystic kidney disease (PKD) without ablating cilia
- Mutating a residue critical for ARL13B's activation of ARL3 suppresses cystic phenotypes in *Pkd1*-dependent cysts

ABSTRACT

Background

Polycystic kidney disease (PKD) is the leading genetic cause of renal failure, resulting in the accumulation of fluid filled cysts and gross enlargement of the kidney. Mutations in *PKD1* or *PKD2*, which encode ciliary polycystin proteins, are the most common cause of PKD. These proteins function in a cilia-dependent cyst activation (CDCA) pathway–one that requires cilia for its pro-cystic function–yet the molecular driver(s) of this pathway are unknown. ARL13B is a regulatory GTPase enriched in cilia with guanine nucleotide exchange factor (GEF) activity and links to renal cystogenesis.

Methods

We use two distinct *Arl13b* mouse alleles to investigate whether ARL13B is a component of the CDCA pathway: *Arl13b*^{V358A} encodes for enzymatically normal ARL13B that is undetectable in cilia, and *Arl13b*^{R79Q} encodes for cilia-localized ARL13B lacking a residue critical for its GEF activity. We used these alleles in a *Pkd1*-deficient adult mouse model, and investigated renal morphology (H&E and cystic index analysis), physiology (blood urea nitrogen measurements), renal fibrosis (picrosirius staining and α-smooth muscle actin levels), renal injury (SOX9

immunofluorescent staining and quantification), and Wnt signaling (β-catenin and cyclin D1 protein levels).

Results

We found that loss of ciliary ARL13B or mutating a single residue critical for its GEF activity suppressed *Pkd1*-dependent cysts. We observed a reduction in kidney size, cystic index, and blood urea nitrogen. We also observed suppression of renal fibrosis, renal injury, and β-catenin and cyclin D1 protein levels.

Conclusions

Our results identify a subcellular location and mechanism driving *Pkd1*-dependent renal cystogenesis. We demonstrate that expression of a critical residue for ARL13B's GEF activity specifically in cilia is a key mechanism of the CDCA pathway driving renal cystogenesis.

Introduction

Autosomal dominant polycystic kidney disease (ADPKD) is the most common monogenic disease and the leading genetic cause of renal failure, affecting an estimated 1:500 to 1:1000 people worldwide[1-4]. Mutations in either *PKD1* or *PKD2* account for over 95% of cases of ADPKD[5-7]. These genes encode the polycystin 1 (PC1) and polycystin 2 (PC2) proteins, which localize to the primary cilium[8-10]. Primary cilia are microtubule-based organelles found on nearly every cell; they provide a privileged compartment linked to several signaling pathways[11-15]. In the kidney, cilia protrude into the lumen of the nephron where they may sense and respond to lumen fluid flow[16-19].

Loss of polycystin function or their exclusion from cilia causes severe renal cyst formation[20,21]. A multitude of aberrant signaling pathways and pathologies including Wnt/β-catenin/cyclin D1 signaling, renal injury, and fibrosis accompany cyst formation in PKD patient samples and genetic animal models[22-33]. Genetic mouse models show that targeting such pathways relieves cyst progression and the affected signaling pathways[28,34-41]. Loss of centrosomal proteins, found at the base of cilia, or loss of cilia themselves results in suppression of severe cystic phenotypes[37,40-42]. The most parsimonious interpretation of these results is the hypothesis of a cilia-dependent cyst activating (CDCA) pathway[37,43,44]. Simultaneous loss of cilia and polycystins suppresses the severe cysts caused by loss of polycystins alone, arguing that polycystin proteins normally function within cilia to inhibit this yet-to-be-identified pro-cystic CDCA pathway[37,43,44]. CDCA pathway components are predicted to localize to cilia, and their intra-cilial loss is expected to suppress polycystin-dependent renal cysts. While discovery-based approaches have identified regulators and targets of the CDCA pathway, the question of the molecular identity of any ciliary drivers of the CDCA pathway remains unanswered[34]. Identifying the molecular components of this pathway will likely identify novel molecular targets for therapy in ADPKD[45].

ARL13B is an ADP-ribosylation factor-like (ARL) family regulatory GTPase enriched in primary cilia whose loss in the kidney causes cysts[46-49]. Loss of *Arl13b* in kidney also leads to a loss of renal cilia[48,49]. In addition to its GTPase activity, ARL13B serves as a guanine nucleotide exchange factor (GEF) for ARL3, another ARL family GTPase that can localize to primary cilia[50,51]. Our work on ARL13B identified mutations that allow us to separate its cilia localization from its known GEF activity[51-57]. *Arl13b*^{V358A} is an engineered gene variant that disrupts ARL13B's RVxP cilia localization motif[52-55]. ARL13B^{V358A} protein is stably expressed and retains GTP binding and GEF activities but is undetectable in cilia[53-55]. *Arl13b*$^{V358A/V358A}$ mice display normal ciliation and cilia length in their kidneys, however they develop mild cystogenesis during development, suggesting ARL13B exhibits distinct ciliary and non-ciliary functions in the kidney[55]. In contrast, the ARL13B^{R79Q} mutation abolishes ARL13B GEF activity for ARL3 *in vitro* without altering its cilia localization, and mice homozygous for this mutation do not develop kidney cysts[51,53,55-58].

The molecular identity of any components of the CDCA has been a mystery in the PKD field. We hypothesize that ciliary ARL13B is a driver in the CDCA pathway. Whereas the complete loss of *Arl13b* causes an ablation of renal cilia, *Arl13b*^{V358A} removes ARL13B from cilia while leaving cilia intact, allowing us to directly test ciliary ARL13B's role in the CDCA pathway to drive renal cystogenesis. The R79Q mutation in ARL13B ablates ARL13B GEF activity for ARL3 *in vitro*[51]; here we use *Arl13b*^{R79Q} mice and demonstrate that ARL13B drives cystogenesis via this critical residue. Lastly, we combined both *Arl13b*^{V358A} and *Arl13b*^{R79Q} alleles, generating mice in which non-ciliary, cellular ARL13B is enzymatically normal, but ciliary ARL13B has mutant GEF activity. These mutants reveal that ARL13B's role in cystogenesis is mediated by the residue controlling its ARL3 GEF activity specifically in renal cilia, implicating these ARLs as major drivers of the pro-cystic CDCA pathway.

Methods

Mouse strains and procedures.

All mice were maintained and cared for in accordance with NIH guidelines and Emory University's Institutional Animal Care and Use Committee (IACUC). All mice were maintained on C57Bl/6J background. *Arl13b* point mutations, including the loss of ciliary ARL13B allele, *Arl13b*^{V358A} (MGI:6256969), and loss of the residue controlling ARL13B's GEF activity for ARL3, *Arl13b*^{R79Q} (MGI:6279301), have been previously described[54-56,59]. Conditional alleles include *Pkd1*^{flox} (MGI:3612341) and *Arl13b*^{flox} (MGI:6107225)[60,61]. Inactivation of conditional floxed alleles was performed using the Pax8^{rtTA} (MGI:3709326) and TetO-Cre (MGI:2679524) transgenes[62,63]. Gene inactivation was achieved by 5 doses of intraperitoneal (IP) injection of 50 mg/kg doxycycline hyclate in water: 3 consecutive daily doses administered at 4 weeks, a fourth dose at six weeks, and a fifth dose at eight weeks as recommended by the Polycystic Kidney Disease Research Resource Consortium. Animals were harvested at 18 weeks as described below unless otherwise indicated.

Animal harvest and tissue processing.

Animals were euthanized by isoflurane inhalation and weighed prior to harvest. Blood was collected by cardiac puncture. Following blood collection, the left renal artery was ligated. The left kidney was removed, weighed, and snap frozen for later processing for protein analysis. Animals were perfused with ice cold PBS followed by 4% paraformaldehyde in PBS. After perfusion, the right kidney was removed, weighed, and further fixed in 4% paraformaldehyde for 24 h before embedding in paraffin following standard procedures.

Blood chemistry.

Blood was collected via cardiac puncture prior to perfusion. Blood was centrifuged at 3500 rpm for 10 min; serum was transferred to a new tube, snap frozen, and stored at -80°C until analysis. Blood urea nitrogen (BUN) analysis was carried out by Emory's Division of Animal Resources (DAR) Diagnostic Services using ACE BUN/Urea Reagent and ACE Creatinine Reagent (Alfa Wassermann), respectively.

Histology.

Paraffin embedded kidneys were sectioned at 8-10 μm. For hematoxylin and eosin (H&E) staining, kidney sections were deparaffinized by exposure to SafeClear (Fisher Scientific 23-314629) in 10 min intervals a total of 3 times, followed by rehydration through a series of decreasing ethanol concentrations for 2 min each (100% ethanol, 100% ethanol, 100% ethanol, 90% ethanol, 70% ethanol, and water). Slides were submerged in Mayer's hematoxylin (Sigma-Aldrich MHS32) for 7 min, rinsed under running tap water for 15 s, then submerged in 90% ethanol for 30 s. Slides were submerged in eosin (Richard-Allan Scientific 7111) for 30 s, then dehydrated through 100% ethanol 4 times, and Safeclear a total of 3 times, then mounted with Cytoseal 60 (Epredia 8310-4). Slides were imaged on an Olympus Nanozoomer slide scanner. Total tissue area was calculated by thresholding in QuPath (v0.6.0)[64]. Cysts were detected by further thresholding on tissue regions with a minimum area of 1500 μm^2 as previously described[65]. Cystic index was calculated as the sum of the cystic area divided by the total tissue area. For Sirius red/fast green staining, kidney sections were deparaffinized by exposure to SafeClear in 5 min intervals a total of 2 times, followed by rehydration through a series of decreasing ethanol concentrations for 2 min each (100%, 100%, 95%, 95%, 70%, 50%, water, water). After rehydration, slides were incubated in 0.04% Fast green FCF (Sigma-Aldrich F7252), 0.1% Direct red 80 (Sigma-Aldrich 365548) in saturated picric aqueous solution (Sigma-

Aldrich P6744) for 15 minutes. Slides were dehydrated in 100% ethanol for 5 min, treated with SafeClear for 10 min, then mounted with Cytoseal 60.

Immunofluorescent Staining.

Paraffin-embedded kidney sections were rehydrated as above and antigen retrieval was performed with 10 mM citrate buffer, pH 6.0 (1.26 mM citric acid monohydrate, Fisher Chemical A104 and 8.74 mM sodium citrate dihydrate, Fisher BioReagents BP327). Following antigen retrieval, slides were blocked in 1% heat inactivated goat serum (MP Biomedicals 2939249) and 0.1% Triton™ X-100 (Fisher BioReagents BP151) in 1x TBS for 1 hr at room temperature. Slides were treated with rabbit anti-SOX9 antibody (1:500, Millipore Cat# AB5535, RRID:AB_2239761) and incubated overnight at 4°C. Slides were washed 3x and incubated with AlexaFluor 647 goat anti-rabbit (1:500, Jackson ImmunoResearch Labs Cat# 111-605-144, RRID:AB_2338078) secondary antibody and Hoechst 33342 (1:5000, Thermo Fisher Scientific Cat# H3570, RRID:AB_3675235) for 1 hr at room temperature. Slides were washed 3x and mounted with ProLong™ Gold Antifade Mountant (Invitrogen P36930). QuPath was used for quantification on 5 or more biological replicates across the entire kidney section in an unbiased manner.

Western blot.

Kidneys were lysed in RIPA Buffer (140 mM NaCl, 10 mM Tris-HCl pH 8.0, 1 mM EDTA, 0.5 mM EGTA, 1% Triton X-100, 0.1% sodium dodecyl sulfate, 0.1% sodium deoxycholate) with Pierce Protease Inhibitor (A32955) and Pierce Phosphatase Inhibitor (88667). Sample concentrations were quantified using Pierce BCA Assay and 40 μg of each sample was loaded onto 10% SDS-PAGE gels. Gels were transferred to 0.2 μm nitrocellulose blotting membranes at 20V for 18 hours. Membranes were blocked in 5% nonfat milk in TBS-T (0.1% Tween-20) for

1 hr at room temperature. Membranes were incubated with mouse anti-HSP90 (1:3000, Santa Cruz Biotechnology Cat# sc-13119, RRID:AB_675659) and rabbit anti-alpha smooth muscle Actin antibody [EPR5368] (1:1000, Abcam Cat# ab124964, RRID:AB_11129103), rabbit anti-b-catenin (1:1000, Thermo Fisher Scientific Cat# 71-2700, RRID:AB_2533982) or rabbit anti-Cyclin D1 [EPR2241] (1:1500, Abcam Cat# ab134175, RRID:AB_2750906) primary antibodies overnight at 4°C. Membranes were washed with TBS-T and incubated with IRDye 680RD donkey anti-mouse (1:10,000, LICORbio Cat# 926-68072, RRID:AB_10953628) and IRDye 800CW donkey anti-rabbit (1:10,000, LICORbio Cat# 925-32213, RRID:AB_2715510) secondary antibodies for 1 hr at room temperature. Membranes were washed with TBS-T and imaged on an Azure Biosystems imager. Densitometry analysis was performed with ImageLab software version 6.1 (Bio-Rad). Analysis was carried out on 3 biological replicates.

Results

Loss of ARL13B from cilia suppresses kidney cyst growth and restores kidney physiology in an adult mouse model of polycystic kidney disease.

The CDCA pathway model of PKD pathogenesis posits that its components are in cilia and that loss of critical pathway components suppresses *Pkd1*-dependent cysts. Ciliary proteins are known to play distinct roles in development and adult, especially in the kidney[18,66]; here we test ARL13B's role in cystogenesis, specifically in an adult model of PKD. To achieve genetic deletion specifically in the kidney epithelium, we used the *Pax8*^{rtTA}; *TetO-Cre* system and began doxycycline induction at 4 weeks of age before harvesting animals at 18 weeks (Fig. 1a, see *Methods*). For simplicity, we abbreviate *Pax8*^{rtTA}; *TetO-Cre* as *PTCre* throughout this text, and we place *PTCre* at the end of each genotype to highlight the meaningful alleles in these experiments. As expected, loss of polycystin 1 (PC1, encoded by *Pkd1*) in single mutant *Pkd1*$^{floxed(fl)/fl}$; *PTCre* animals led to an increase in kidney weight to body weight (KW:BW), cystic index (cyst area divided by total kidney area), and blood urea nitrogen (BUN) levels compared

to control animals (Fig. 1b-e). Since our experimental *Arl13b* mutant alleles were tested over the floxed allele, we next tested whether loss of one copy of *Arl13b* impacted cystic phenotypes. The loss of one copy of *Arl13b* had a mild impact on the *Pkd1* cystic phenotype: *Pkd1*$^{fl/fl}$; *Arl13b*$^{fl/+}$; *PTCre* animals showed a decrease in KW:BW and BUN compared to *Pkd1*$^{fl/fl}$; *PTCre* single mutant animals, while cystic index remained elevated (Fig. 1b-e). To test whether ciliary ARL13B is a driver of the CDCA pathway, we generated *Pkd1* mice lacking ARL13B specifically in cilia of renal epithelial cells. To do so, we combined the *Arl13b*^{V358A} allele, in which ARL13B is undetectable in cilia, with the conditional null *Arl13b*^{fl} allele in *Pkd1*$^{fl/fl}$ animals. Loss of ciliary ARL13B in single mutant adult *Arl13b*$^{V358A/fl}$; *PTCre* animals did not alter kidney size, morphology, or physiology compared with control animals (Fig. 1b-e). In contrast, double mutant *Pkd1*$^{fl/fl}$; *Arl13b*$^{V358A/fl}$; *PTCre* animals exhibited a suppression of the severe *Pkd1*$^{fl/fl}$; *PTCre* cystic phenotype, resembling control animals for KW:BW and BUN levels (Fig. 1b-c,e). While cystic index was elevated in *Pkd1*$^{fl/fl}$; *Arl13b*$^{V358A/fl}$; *PTCre* double mutants compared to controls (Fig. 1d), the increase was driven by a few large, focal cysts with most of the tissue exhibiting normal histology (Fig. 1b). Overall, our results indicate that ciliary ARL13B drives renal cystogenesis in *Pkd1*-deficient mouse kidneys.

Loss of ciliary ARL13B suppresses fibrosis in an adult PKD mouse model.

Cystogenesis coincides with an accumulation of renal fibrosis, a hallmark of PKD[30,32,33]. As cystic disease progresses, concurrent fibrosis occurs in both mouse models and clinical samples[30,32,33]. We investigated renal fibrosis in our cohorts using Sirius red to stain collagen in fibrotic regions and fast green as a counterstain for non-collagenous regions. We observed Sirius red staining throughout *Pkd1*$^{fl/fl}$; *PTCre* single mutant kidneys (Fig. 2a). The additional loss of one copy of *Arl13b* (*Pkd1*$^{fl/fl}$; *Arl13b*$^{fl/+}$; *PTCre*) did not reduce this phenotype (Fig. 2a). Independent loss of ciliary ARL13B (*Arl13b*$^{V358A/fl}$; *PTCre*) did not result in any observable

fibrotic regions (Fig. 2a). *Pkd1*$^{fl/fl}$; *Arl13b*$^{V358A/fl}$; *PTCre* kidneys displayed a marked reduction in fibrosis compared with *Pkd1*$^{fl/fl}$; *PTCre* single mutant kidneys, with most of the kidney free from fibrosis and only small localized fibrotic regions adjacent to cysts, (Fig. 2a).

Renal fibrosis is characterized by elevated levels of α-smooth muscle actin (αSMA), a marker of myofibroblasts[33]. We observed an increase in αSMA protein levels in kidney lysates from *Pkd1*$^{fl/fl}$; *PTCre* single mutant kidneys compared to control kidneys (Fig. 2b, c). The αSMA levels in *Pkd1*$^{fl/fl}$; *Arl13b*$^{fl/+}$; *PTCre* mutant kidney lysates were also elevated, although the elevated levels were not statistically different from *Arl13b*$^{V358A/fl}$; *PTCre* single mutant or control kidney lysates (Fig. 2b, c). *Pkd1*$^{fl/fl}$; *Arl13b*$^{V358A/fl}$; *PTCre* double mutant animals displayed similar αSMA levels to control animals, indicating a suppression of the fibrotic phenotype observed in *Pkd1*$^{fl/fl}$; *PTCre* single mutants (Fig. 2b, c). While Sirius red staining indicated isolated regions of fibrosis lining the cystic epithelium in our suppression model, the reduction of αSMA levels in kidney lysates indicates that most of the kidney was free from fibrosis. Together, these results indicate that combined loss of PC1 and ciliary exclusion of ARL13B reduced the severe fibrosis seen in loss of PC1 alone.

Loss of ciliary ARL13B suppresses renal injury in an adult PKD mouse model.

In addition to fibrosis, renal injury is a feature of PKD, and SOX9^{+} nuclei are indicative of injury in the renal epithelium[25,27,67,68]. We observed a significant increase in SOX9^{+} nuclei in *Pkd1*$^{fl/fl}$; *PTCre* single mutant kidneys compared to control kidneys (Fig. 2d,e). Loss of ciliary ARL13B alone (*Arl13b*$^{V358A/fl}$; *PTCre*) showed the same percentage of SOX9^{+} nuclei as controls (Fig. 2d,e). In contrast, both *Pkd1*$^{fl/fl}$; *Arl13b*$^{V358A/fl}$; *PTCre* double mutant mice and *Pkd1*$^{fl/fl}$; *Arl13b*$^{fl/+}$; *PTCre* mutant mice had SOX9^{+} nuclei levels comparable to control animals, indicating suppression of the renal injury observed in PC1 single mutant animals (Fig. 2d, e). Loss of one

copy of wild-type *Arl13b* or loss of ciliary ARL13B suppressed the injury observed in *Pkd1*-deleted cystic kidneys. These results indicate that renal injury depends on *Arl13b*.

Ciliary ARL13B mediates Wnt signaling in an adult PKD mouse model.

Elevated Wnt/β-catenin/cyclin D1 signaling promotes renal cystogenesis in PKD mouse models[22-24,69]. To assess whether ciliary ARL13B modulates Wnt signaling in *Pkd1*-dependent cystic kidneys, we immunoblotted kidney lysates for β-catenin and cyclin D1 protein levels (Fig. 3a). We observed a significant increase in both β-catenin and its transcriptional target cyclin D1 in *Pkd1*$^{fl/fl}$; *PTCre* single mutant kidneys compared to control kidneys (Fig. 3a-c). Loss of one copy of *Arl13b* (*Pkd1*$^{fl/fl}$; *Arl13b*$^{fl/+}$; *PTCre*) suppressed the increased β-catenin levels but not the increased cyclin D1 levels observed in *Pkd1*$^{fl/fl}$; *PTCre* single mutant kidneys (Fig. 3a-c). Loss of ciliary ARL13B alone (*Arl13b*$^{V358A/fl}$; *PTCre*) did not cause changes to β-catenin or cyclin D1 levels compared to control kidney lysates (Fig. 3a-c). *Pkd1*$^{fl/fl}$; *Arl13b*$^{V358A/fl}$; *PTCre* double mutant kidneys exhibited β-catenin protein levels comparable to control kidney lysates, indicating a complete reversal of the increase observed in *Pkd1*$^{fl/fl}$; *PTCre* kidney lysates (Fig. 3a,b). In contrast, *Pkd1*$^{fl/fl}$; *Arl13b*$^{V358A/fl}$; *PTCre* kidneys exhibited a partial reduction in cyclin D1 levels compared to *Pkd1*$^{fl/fl}$; *PTCre* but not to levels seen in control kidneys (Fig. 3a,c). Overall, these results indicate that loss of ciliary ARL13B attenuates Wnt/β-catenin/cyclin D1 signaling in an adult PKD mouse model.

Ciliary ARL13B's GEF activity for ARL3 is a likely driver of kidney cystogenesis *in vivo*.

In addition to its GTPase activity, ARL13B also possesses GEF activity for ARL3, another ARL family GTPase that can localize to cilia[50,51,53,57,58]. Given that loss of ciliary ARL13B suppressed *Pkd1*-dependent cysts (*Pkd1*$^{fl/fl}$; *Arl13b*$^{V358A/fl}$; *PTCre*), we asked whether the residue that controls ARL13B's GEF activity also suppressed these cysts. We used a mouse expressing

ARL13B^{R79Q}, a mutant form of ARL13B that localizes to cilia yet cannot activate ARL3 *in vitro*[51,53,56]. Loss of the residue critical for ARL13B GEF activity alone in *Arl13b*$^{R79Q/fl}$; *PTCre* single mutant animals did not result in changes to KW:BW, cystic index, or BUN levels compared to control animals (Fig. 4a-d). Simultaneous loss of *Pkd1* with this *Arl13b* mutant (*Pkd1*$^{fl/fl}$; *Arl13b*$^{R79Q/fl}$; *PTCre*) suppressed the increased KW:BW, cystic index, and BUN levels observed in *Pkd1*$^{fl/fl}$; *PTCre* single mutants (Fig. 4a-d). We also examined *Pkd1*$^{fl/fl}$; *Arl13b*$^{R79Q/R79Q}$; *PTCre* animals and observed suppressed KW:BW, cystic index, and BUN levels compared to *Pkd1*$^{fl/fl}$; *PTCre* single mutant animals (Fig. 4a-d). Together, these results indicate that a residue essential for ARL13B's GEF activity for ARL3 is required for renal cystogenesis when *Pkd1* is lost.

To explore whether ARL13B drives cystic phenotypes via its GEF activity specifically in cilia, we combined the *Arl13b*^{R79Q} and *Arl13b*^{V358A} alleles. The ciliary ARL13B in these *Arl13b*$^{R79Q/V358A}$ mice lacks the residue controlling GEF activity for ARL3, while cellular ARL13B retains enzymatic activities (Fig. 6, right). *Pkd1*$^{fl/fl}$; *Arl13b*$^{R79Q/V358A}$; *PTCre* mice exhibited KW:BW, cystic index, and BUN levels comparable to control animals, indicating that GEF mutant ARL13B^{R79Q} in cilia suppresses the cysts caused by loss of *Pkd1* alone (Fig. 4a-d). Taken together, these data indicate the R79 residue controlling ARL13B GEF activity for ARL3 drives *Pkd1*-dependent cystogenesis from within cilia.

Pkd1-deficient kidneys expressing _Arl13b_^{R79Q} do not develop renal fibrosis.

Since loss of ciliary ARL13B suppressed fibrosis in *Pkd1* mutant kidneys (Fig. 2a), we asked whether this suppression depended on the residue critical for ARL13B's GEF activity. We observed levels of Sirius red staining in *Arl13b*$^{R79Q/fl}$; *PTCre* single mutant kidneys comparable to controls (Fig. 5a). As we observed in loss of ciliary ARL13B (*Pkd1*$^{fl/fl}$; *Arl13b*$^{V358A/fl}$; *PTCre*, Fig. 2a), ARL13B^{R79Q} expression throughout the cell (*Pkd1*$^{fl/fl}$; *Arl13b*$^{R79Q/R79Q}$; *PTCre*) or GEF

mutant ARL13B in cilia and enzymatically normal ARL13B in the cell (*Pkd1*$^{fl/fl}$; *Arl13b*$^{R79Q/V358A}$; *PTCre*) suppressed the severe fibrotic phenotype caused by loss of *Pkd1* alone (Fig. 5a).

We next looked at αSMA in lysates from these models. Single mutant *Pkd1*$^{fl/fl}$; *PTCre* kidney lysates displayed a nearly two-fold increase in αSMA compared to control kidney lysates (Fig. 5b,c). Loss of the residue controlling ARL13B GEF activity for ARL3 in *Arl13b*$^{R79Q/fl}$; *PTCre* mice did not cause any changes in αSMA protein levels compared to control kidney lysates (Fig. 5b,c). *Pkd1*$^{fl/fl}$; *Arl13b*$^{R79Q/fl}$; *PTCre*, *Pkd1*$^{fl/fl}$; *Arl13b*$^{R79Q/R79Q}$; *PTCre* and *Pkd1*$^{fl/fl}$; *Arl13b*$^{R79Q/V358A}$; *PTCre* kidney lysates exhibited levels comparable to control kidney lysates (Fig. 5b,c). These results indicate that ARL13B^{R79Q} expression specifically in cilia suppresses the severe cystic phenotypes and accompanying renal fibrosis caused by loss of *Pkd1* alone.

Renal injury in a *Pkd1*-dependent mouse model requires the residue of ARL13B controlling its ARL3 GEF activity.

To investigate renal injury in these mice, we quantified SOX9^{+} nuclei. Similar to our previous results, we observed an increase in SOX9^{+} nuclei in *Pkd1*$^{fl/fl}$; *PTCre* mutant mice (Fig. 5d, e), indicative of renal epithelial cell injury. Kidney sections from *Arl13b*$^{R79Q/fl}$; *PTCre* mice showed a similar percentage of SOX9^{+} nuclei compared to control sections (Fig. 5d, e). The SOX9^{+} increase in *Pkd1*$^{fl/fl}$; *PTCre* mutant kidneys was suppressed in *Pkd1*$^{fl/fl}$; *Arl13b*$^{R79Q/fl}$; *PTCre*, *Pkd1*$^{fl/fl}$; *Arl13b*$^{R79Q/R79Q}$; *PTCre* and *Pkd1*$^{fl/fl}$; *Arl13b*$^{R79Q/V358A}$; *PTCre* kidneys, which showed SOX9^{+} nuclei numbers comparable to control kidneys (Fig. 5d, e). Taken together, these results indicate that expression of ARL13B^{R79Q} specifically in cilia suppresses the severe cystic phenotypes and associated fibrosis and injury observed when PC1 is lost.

***Arl13b*^{R79Q} suppresses Wnt signaling in *Pkd1*-null kidneys.**

To examine whether ARL13B acts via its GEF activity to modulate Wnt signaling, we looked at β-catenin and cyclin D1 levels in *Arl13b*^{R79Q} animals. *Pkd1*$^{fl/fl}$; *PTCre* kidney lysates exhibited a five- and three-fold increase in β-catenin and cyclin D1 levels compared to control kidney lysates, respectively. *Arl13b*$^{R79Q/fl}$; *PTCre* mice expressed β-catenin and cyclin D1 levels comparable to control animals (Fig. 5f-h). *Pkd1*$^{fl/fl}$; *Arl13b*$^{R79Q/fl}$; *PTCre* double mutant mice suppressed the increase in both β-catenin and cyclin D1 protein levels observed in *Pkd1*$^{fl/fl}$; *PTCre* single mutants back to control levels (Fig. 5f-h). *Pkd1*$^{fl/fl}$; *Arl13b*$^{R79Q/R79Q}$; *PTCre* and *Pkd1*$^{fl/fl}$; *Arl13b*$^{R79Q/V358A}$; *PTCre* mice suppressed β-catenin to control levels but did not suppress cyclin D1, which remained significantly elevated compared to control samples (Fig. 5f-h). These results indicate that the residue essential for ARL13B GEF activity is also required for elevated Wnt/β-catenin/Cyclin D1 signaling in *Pkd1* mouse models. Additionally, we see the phenotype is dose-dependent since *Pkd1*$^{fl/fl}$; *Arl13b*$^{R79Q/R79Q}$; *PTCre* and *Pkd1*$^{fl/fl}$; *Arl13b*$^{R79Q/V358A}$; *PTCre* kidneys have elevated cyclin D1 protein levels, while *Pkd1*$^{fl/fl}$; *Arl13b*$^{R79Q/fl}$; *PTCre* kidneys have cyclin D1 protein levels comparable to control kidneys. In summary, *Pkd1*$^{fl/fl}$; *Arl13b*$^{R79Q/V358A}$; *PTCre* mice exhibited diminished renal cystic phenotypes compared to *Pkd1*$^{fl/fl}$; *PTCre* single mutant animals.

Discussion

Primary cilia have long been implicated in PKD pathogenesis[13,16,70]. Work in mouse models has strongly suggested the existence of a cilia-dependent cyst activation (CDCA) pathway that drives cystic disease, yet its molecular identity has remained a black box for over a decade[37,44]. The CDCA pathway hypothesis made two predictions borne out by our data: that the CDCA components are in cilia and that their intra-cilial loss of function suppresses polycystin-dependent renal cysts. While this CDCA pathway is one interpretation of suppression in mouse models, it is very difficult to prove this pathway exists until it is properly identified. Our

work supports the CDCA model and provides a molecular entry point from which to dissect the CDCA pathway. First, we found that loss of ciliary ARL13B in *Pkd1*$^{fl/fl}$; *Arl13b*$^{V358A/fl}$; *PTCre* double mutants suppressed the severe cystic phenotype seen in *Pkd1*$^{fl/fl}$; *PTCre* single mutant kidneys, indicating ARL13B functions in cilia to drive renal cystogenesis. Second, we showed *Pkd1*$^{fl/fl}$; *Arl13b*$^{R79Q/fl}$; *PTCre* mutants also suppressed the severe cystic phenotype caused by loss of PC1 in *Pkd1*$^{fl/fl}$; *PTCre* kidneys, revealing ARL13B drives renal cystogenesis via the residue controlling its ARL3 GEF activity. Lastly, we observed *Pkd1*$^{fl/fl}$; *Arl13b*$^{R79Q/V358A}$; *PTCre* mutant mice suppressed the severe cystic phenotypes in *Pkd1*$^{fl/fl}$; *PTCre* mutant mice. These results indicate that ARL13B drives renal cystogenesis via the residue controlling its GEF activity for ARL3, specifically in cilia (Fig. 6). Taken together, these data reveal ARL13B to be a driver of the pro-cystic CDCA pathway in an orthologous PKD mouse model. While there are currently no known inhibitors of ARL13B's GTPase or GEF activity, nor of ARL3's GTPase activity, our data suggest these enzymatic activities are prime targets for treatment strategies.

PC1 and PC2 form a transmembrane complex that localizes to the primary cilium where it functions to inhibit renal cystogenesis[71,72]. In mouse, PC2 must be in cilia to function as *Pkd2* mutants encoding for non-ciliary PC2 phenocopy *Pkd2*-null mutants[20]. These results clearly show that PC2 functions in cilia, consistent with ARL13B functioning in cilia to drive renal cystogenesis. However, whether ciliary ARL13B drives *Pkd2*-dependent cystogenesis would need to be formally tested.

We show mouse ARL13B functions in the CDCA pathway via its arginine at amino acid position 79, which is the residue required for its GEF activity *in vitro*[51]. Thus, our data suggest, but do not prove, that ARL13B functions via its GEF activity for ARL3 in the CDCA pathway *in vivo*. While purified mammalian ARL13B^{R79Q} is unable to activate ARL3 *in vitro*, we cannot rule out the possibility of another protein acting as a GEF for ARL3 *in vivo* and have no assay to measure ARL3 activity *in vivo*. Future work directly manipulating ARL3's activation state will be

needed to directly test ARL3's role in mediating suppression of renal cystogenesis. Our results reveal ciliary ARL13B's GEF activity for ARL3 is a likely mechanism of the CDCA pathway driving cystogenesis.

We note that while most kidney tissue in the genetic suppression models retains normal morphology and physiology, there are isolated "breakthrough" cysts. The most likely explanation for these sporadic cysts is discordant recombination of the floxed alleles as reported for other loci[73,74]; inefficient or delayed recombination of the *Arl13b*^{fl} allele may have permitted *Pkd1*-dependent cystogenesis to initiate. Alternatively, the breakthrough cysts could reflect ARL13B's cellular GTPase activity playing a minor role in modulating the CDCA pathway in *Pkd1*-mutant cysts. Regardless, we observed grossly normal morphology and renal physiology in *Pkd1*-deficient kidneys, whether cysts were suppressed with *Arl13b*^{V358A}, *Arl13b*^{R79Q}, or a combination of the two alleles.

Our data are consistent with several previous findings. Loss of the cilia trafficking protein TULP3 suppressed the severe cystic phenotype caused by loss of PC1 alone in adult mouse models of PKD[41]. TULP3 is required for ARL13B's ciliary localization in the kidney[41,75]. Our findings suggest that TULP3 mediates cyst suppression via ciliary ARL13B. Additionally, both TULP3 and ARL13B regulate Hedgehog (Hh) signaling, which is implicated in regulating kidney cystogenesis[76-78]. While Hh signaling inhibition attenuates cystogenesis in *in vitro* and *ex vivo* models[76-78], recent work argues that Hh signaling is dispensable for cyst progression in *in vivo* mouse models[79,80]. Despite complete loss of ARL13B misregulating Hh signaling, both ARL13B^{V358A} and ARL13B^{R79Q} permit normal Hh signaling[53,54,56]. Thus, our findings are consistent with ARL13B driving cystogenesis independent of its regulation of Hh signaling. Finally, we showed that β-catenin and cyclin D1 are elevated in *Pkd1* mutant kidneys, implicating aberrant Wnt signaling in renal cystogenesis. Loss of ciliary ARL13B or the residue controlling its GEF activity for ARL3 completely rescued β-catenin expression back to control

levels but only partially rescued the expression of cyclin D1. These findings suggest that ARL13B plays a non-ciliary role, independent of its R79 residue, to regulate cyclin D1 signaling in *Pkd1* mutant kidneys.

Since the CDCA was first postulated, much work has focused on discovering the molecular identity of a ciliary driver of PKD pathogenesis. Many exciting candidates emerged from these studies, including *Tulp3*, *Glis2*, and *Ankmy2*[34,41,42], however none of their encoded proteins have been found in cilia. Despite initial reports of GLIS2 localization to cilia, the majority of the protein localizes to the nucleus[34]. TULP3 and ANKMY2 regulate the localization of several ciliary proteins[41,42,75,81-85]. In the kidney, TULP3 traffics ARL13B into cilia, and its loss suppresses severe cystic *Pkd1*-dependent phenotypes in adult mice[41,75]. Our data argue that TULP3 acts through ARL13B and ARL13B likely acts through ARL3 to drive cystogenesis *in vivo*. In conclusion, our work indicates that ARL13B is a major component of the CDCA pathway and that this mechanism largely depends on the residue required for ARL13B GEF activity for ARL3 in cilia. These results provide the field a molecular foothold for discovering additional CDCA components and their mechanisms of action, as well as dissect other ciliary mechanisms driving polycystic kidney disease.

Disclosures

The authors declare no competing interests and no disclosures.

Funding

This work was supported by the National Institutes of Health: Institutional Research and Career Development Award (IRACDA) K12GM000680, F32DK127848, and K01DK140605 to REVS; the Summer Undergraduate Program in Emory Renal Research (SUPERR), R25DK101390 to AKF; and R35GM148416 and R01DK128902 to TC.

Acknowledgments

H&E slide scanning in this publication was supported in part by the Cancer Tissue and Pathology Shared Resource of Winship Cancer Institute of Emory University and NIH/NCI under award number P30CA138292. This work was supported by the Emory University Integrated Cellular Imaging Core Facility (RRID:SCR_023534). The content is solely the responsibility of the authors and does not necessarily reflect the official views of the National Institute of Health. We are grateful to Sarah Bay and members of the Caspary lab for feedback, comments, and suggestions in the preparation of this manuscript.

Figure 1: Loss of ciliary ARL13B suppresses severe cystic PC1-deficient phenotypes.

(**a-e**) Simultaneous loss of ciliary ARL13B and polycystin 1 (PC1, encoded by *Pkd1*) rescues severe cystic phenotypes caused by loss of PC1 alone in an adult *Pkd1*-mouse model. (**a**) Schematic representation of Cre induction and animal harvest experiments. Animals were injected with 5 doses of doxycycline beginning at 4 weeks of age and harvested at 18 weeks of age. (**b**) Representative hematoxylin and eosin (H&E) staining reveals gross kidney morphology of the indicated genotypes. Scale bar is 2 mm. (**c**) Quantitative representation of the total kidney weight to body weight ratio. (**d**) Cystic index (cyst area divided by total area of kidney cross section) reveals structural insights into kidney morphology. (**e**) Blood urea nitrogen (BUN) shows functional renal physiology. Symbols in the graphs **c-e** correspond to the genotypes indicated in **b**, with male mice represented by closed symbols female mice represented by open symbols. Data presented as mean ± SEM; sample size indicated below each graph. Statistical analysis is one-way ANOVA with Tukey's multiple comparisons test. Asterisk (*****) indicates significant difference ($p < 0.05$) from control; dagger (**†**) indicates significant difference ($p < 0.05$) from *Pkd1*$^{fl/fl}$; *PTCre* single mutants.

Figure 2: Loss of ciliary ARL13B suppresses fibrosis and injury in adult *Pkd1* mouse models.

Simultaneous loss of ciliary ARL13B and PC1 rescues fibrosis and injury caused by loss of PC1 alone, as indicated by morphological (**a**), molecular (**b, c**), and cellular (**d, e**) analysis. (**a**) Sirius red and fast green staining reveals fibrosis in cyst-adjacent areas. (**b, c**) Western blot and densitometry analysis of the myofibroblast marker α-smooth muscle actin (α-SMA) in kidney lysates ($n = 3$). (**d, e**) Quantification and images of renal injury marker SOX9 in kidney sections ($n = 5$-6). Scale bars are 200 μm (a) and 50 μm (e). Genotypes in **b-e** correspond to symbol colors and shapes indicated in **a**. Data presented as mean ± SEM. Statistical analysis is one-

way ANOVA with Tukey's multiple comparisons test. Asterisk (*) indicates significant difference ($p < 0.05$) from control; dagger (**†**) indicates significant difference ($p < 0.05$) from *Pkd1*$^{fl/fl}$; *PTCre* single mutants.

Figure 3: Ciliary ARL13B drives Wnt signaling in adult *Pkd1* mouse models.

(**a**) Western blot of Wnt signaling components β-catenin and cyclin D1 in kidney lysates. (b, c) Densitometry analysis of (**b**) β-catenin and (**c**) cyclin D1 ($n = 3$). Genotypes in **b, c** correspond to symbol colors and shapes indicated in **a**. Data presented as mean ± SEM. Statistical analysis is one-way ANOVA with Tukey's multiple comparisons test. Asterisk (*) indicates significant difference ($p < 0.05$) from control; dagger (**†**) indicates significant difference ($p < 0.05$) from *Pkd1*$^{fl/fl}$; *PTCre* single mutants.

Figure 4: *Arl13b*^{R79Q} suppresses severe cystic *Pkd1*-phenotypes.

(**a-d**) Kidney morphology and physiology reveal that expression of ARL13B^{R79Q} rescues the severe cystic phenotypes caused by loss of PC1. (**a**) Representative hematoxylin and eosin (H&E) staining reveals gross kidney morphology of the indicated genotypes. Scale bar is 2 mm. (**b**) Quantitative representation of the total kidney weight to body weight ratio. (**c**) Cystic index (cyst area divided by total area of kidney cross section) reveals structural insights into kidney morphology. (**d**) Blood urea nitrogen (BUN) shows functional renal physiology. Genotypes in **b-d** correspond to symbol colors and shapes indicated in **a**. Closed symbols indicate male mice and open symbols indicate female mice. Data presented as mean ± SEM; sample size indicated below each graph. Statistical analysis is one-way ANOVA with Tukey's multiple comparisons test. Asterisk (*) indicates significant difference ($p < 0.05$) from control; dagger (**†**) indicates significant difference ($p < 0.05$) from *Pkd1*$^{fl/fl}$; *PTCre* single mutants.

Figure 5: ARL13B^{R79Q} suppresses fibrosis, injury, and Wnt signaling in *Pkd1*-deficient kidneys.

Morphological, molecular, and cellular analysis reveal that ARL13B^{R79Q} rescues fibrosis, injury, and Wnt signaling caused by loss of PC1. (**a**) Sirius red and fast green staining reveals fibrosis in cyst-adjacent areas. (**b, c**) Western blot and densitometry analysis of the myofibroblast marker α-SMA in kidney lysates ($n = 3$). (**d, e**) Quantification and images of renal injury marker SOX9 in kidney sections ($n = 6$). (**f**) Western blot of Wnt signaling components β-catenin and cyclin D1 in kidney lysates. (**g**, **h**) Densitometry analysis of (**g**) β-catenin and (**h**) cyclin D1 ($n = 3$). Scale bars are 200 μm (**a**) and 50 μm (**e**). Genotypes in **b-h** correspond to symbol colors and shapes indicated in **a**. Data presented as mean ± SEM. Statistical analysis is one-way ANOVA with Tukey's multiple comparisons test. Asterisk (*****) indicates significant difference ($p < 0.05$) from control; dagger (**†**) indicates significant difference ($p < 0.05$) from *Pkd1*$^{fl/fl}$; *PTCre* single mutants.

Figure 6: Ciliary ARLs are major drivers of the pro-cystic CDCA pathway.

Our data show that ciliary ARL13B drives renal cystogenesis in *Pkd1*-deficient kidneys. ARL13B, ARL3, and the polycystin complex PC1/PC2 localize to primary cilia. Under normal conditions, PC1/2 inhibit a pro-cystic CDCA pathway, preventing cystogenesis (**left**). Loss of PC1 (encoded by *Pkd1*) relieves inhibition of the CDCA pathway, resulting in severe cystic phenotypes (**center**). Mutation of the R79 residue critical to ARL13B's GEF activity for ARL3 does not alter ARL13B's localization to cilia. Loss of this residue specifically in cilia (R79Q) while retaining enzymatically normal ARL13B in the cell (V358A) suppresses the severe cystic phenotype caused by loss of PC1 alone (**right**), indicating that ARL13B's ciliary GEF activity for ARL3 is a major driver of the pro-cystic CDCA pathway.

References

1. Willey, C., Kamat, S., Stellhorn, R. & Blais, J. Analysis of Nationwide Data to Determine the Incidence and Diagnosed Prevalence of Autosomal Dominant Polycystic Kidney Disease in the USA: 2013–2015. *Kidney Diseases* **5**, 107–117 (2019).
2. Willey, C.J. *et al.* Prevalence of autosomal dominant polycystic kidney disease in the European Union. *Nephrology Dialysis Transplantation* **32**, 1356–1363 (2016).
3. Bergmann, C. *et al.* Polycystic kidney disease. *Nat Rev Dis Primers* **4**, 50 (2018).
4. Lanktree, M.B. *et al.* Prevalence Estimates of Polycystic Kidney and Liver Disease by Population Sequencing. *Journal of the American Society of Nephrology* **29**, 2593–2600 (2018).
5. Lanktree, M.B., Haghighi, A., di Bari, I., Song, X. & Pei, Y. Insights into Autosomal Dominant Polycystic Kidney Disease from Genetic Studies. *Clinical Journal of the American Society of Nephrology*, CJN.02320220 (2020).
6. Cornec-Le Gall, E., Alam, A. & Perrone, R.D. Autosomal dominant polycystic kidney disease. *Lancet* **393**, 919–935 (2019).
7. Cornec-Le Gall, E., Torres, V.E. & Harris, P.C. Genetic Complexity of Autosomal Dominant Polycystic Kidney and Liver Diseases. *J Am Soc Nephrol* **29**, 13–23 (2018).
8. Hughes, J. *et al.* The polycystic kidney disease 1 (PKD1) gene encodes a novel protein with multiple cell recognition domains. *Nat Genet* **10**, 151–60 (1995).
9. Mochizuki, T. *et al.* PKD2, a gene for polycystic kidney disease that encodes an integral membrane protein. *Science* **272**, 1339–42 (1996).
10. The International Polycystic Kidney Disease Consortium. Polycystic kidney disease: the complete structure of the PKD1 gene and its protein. The International Polycystic Kidney Disease Consortium. *Cell* **81**, 289–98 (1995).
11. Huangfu, D. *et al.* Hedgehog signalling in the mouse requires intraflagellar transport proteins. *Nature* **426**, 83–7 (2003).
12. Barr, M.M. & Sternberg, P.W. A polycystic kidney-disease gene homologue required for male mating behaviour in C. elegans. *Nature* **401**, 386–9 (1999).
13. Pazour, G.J. *et al.* Chlamydomonas IFT88 and its mouse homologue, polycystic kidney disease gene tg737, are required for assembly of cilia and flagella. *J Cell Biol* **151**, 709–18 (2000).
14. Anvarian, Z., Mykytyn, K., Mukhopadhyay, S., Pedersen, L.B. & Christensen, S.T. Cellular signalling by primary cilia in development, organ function and disease. *Nature Reviews Nephrology* **15**, 199–219 (2019).
15. Garcia-Gonzalo, F.R. *et al.* Phosphoinositides Regulate Ciliary Protein Trafficking to Modulate Hedgehog Signaling. *Dev Cell* **34**, 400–409 (2015).
16. Yoder, B.K., Hou, X. & Guay-Woodford, L.M. The polycystic kidney disease proteins, polycystin-1, polycystin-2, polaris, and cystin, are co-localized in renal cilia. *J Am Soc Nephrol* **13**, 2508–16 (2002).
17. Andrews, P.M. & Porter, K.R. A scanning electron microscopic study of the nephron. *Am J Anat* **140**, 81–115 (1974).
18. Davenport, J.R. *et al.* Disruption of intraflagellar transport in adult mice leads to obesity and slow-onset cystic kidney disease. *Curr Biol* **17**, 1586–94 (2007).
19. Zhang, Q., Taulman, P.D. & Yoder, B.K. Cystic Kidney Diseases: All Roads Lead to the Cilium. *Physiology* **19**, 225–230 (2004).
20. Walker, R.V. *et al.* Ciliary exclusion of Polycystin-2 promotes kidney cystogenesis in an autosomal dominant polycystic kidney disease model. *Nat Commun* **10**, 4072 (2019).

21. Franco, I. *et al.* Phosphoinositide 3-Kinase-C2alpha Regulates Polycystin-2 Ciliary Entry and Protects against Kidney Cyst Formation. *J Am Soc Nephrol* **27**, 1135–44 (2016).
22. Kim, S. *et al.* The polycystin complex mediates Wnt/Ca2+ signalling. *Nature Cell Biology* **18**, 752–764 (2016).
23. Conduit, S.E. *et al.* β-catenin ablation exacerbates polycystic kidney disease progression. *Human Molecular Genetics* **28**, 230–244 (2018).
24. Lee, E.J. *et al.* TAZ/Wnt-β-catenin/c-MYC axis regulates cystogenesis in polycystic kidney disease. *Proceedings of the National Academy of Sciences* **117**, 29001–29012 (2020).
25. Leonhard, W.N. *et al.* Scattered Deletion of PKD1 in Kidneys Causes a Cystic Snowball Effect and Recapitulates Polycystic Kidney Disease. *Journal of the American Society of Nephrology* **26**, 1322–1333 (2015).
26. Wang, Q. *et al.* Adenylyl cyclase 5 deficiency reduces renal cyclic AMP and cyst growth in an orthologous mouse model of polycystic kidney disease. *Kidney International* **93**, 403–415 (2018).
27. Zimmerman, K.A. *et al.* Tissue-Resident Macrophages Promote Renal Cystic Disease. *J Am Soc Nephrol* (2019).
28. Wei, Z. *et al.* Anks3 mediates cilia dependent polycystin signaling and is essential for adult kidney homeostasis. *bioRxiv*, 2025.04.22.649832 (2025).
29. Chang, M.Y. *et al.* Haploinsufficiency of Pkd2 is associated with increased tubular cell proliferation and interstitial fibrosis in two murine Pkd2 models. *Nephrology Dialysis Transplantation* **21**, 2078–2084 (2006).
30. Song, C.J., Zimmerman, K.A., Henke, S.J. & Yoder, B.K. Inflammation and Fibrosis in Polycystic Kidney Disease. in *Kidney Development and Disease* (ed. Miller, R.K.) 323–344 (Springer International Publishing, Cham, 2017).
31. Dong, K. *et al.* Renal plasticity revealed through reversal of polycystic kidney disease in mice. *Nature Genetics* **53**, 1649–1663 (2021).
32. Lantinga-van Leeuwen, I.S. *et al.* Lowering of Pkd1 expression is sufficient to cause polycystic kidney disease. *Hum Mol Genet* **13**, 3069–77 (2004).
33. Jiang, S.-T. *et al.* Defining a Link with Autosomal-Dominant Polycystic Kidney Disease in Mice with Congenitally Low Expression of *Pkd1*. *The American Journal of Pathology* **168**, 205–220 (2006).
34. Zhang, C. *et al.* Glis2 is an early effector of polycystin signaling and a target for therapy in polycystic kidney disease. *Nature Communications* **15**, 3698 (2024).
35. He, J. *et al.* Inhibiting Focal Adhesion Kinase Ameliorates Cyst Development in Polycystin-1–Deficient Polycystic Kidney Disease in Animal Model. *Journal of the American Society of Nephrology* **32**, 2159–2174 (2021).
36. Lee, K., Boctor, S., Barisoni, L.M.C. & Gusella, G.L. Inactivation of Integrin-β1 Prevents the Development of Polycystic Kidney Disease after the Loss of Polycystin-1. *Journal of the American Society of Nephrology* **26**, 888–895 (2015).
37. Ma, M., Tian, X., Igarashi, P., Pazour, G.J. & Somlo, S. Loss of cilia suppresses cyst growth in genetic models of autosomal dominant polycystic kidney disease. *Nat Genet* **45**, 1004–12 (2013).
38. Zhang, C. *et al.* Cyclin-Dependent Kinase 1 Activity Is a Driver of Cyst Growth in Polycystic Kidney Disease. *Journal of the American Society of Nephrology*, ASN.2020040511 (2020).
39. Kraus, A. *et al.* P2Y2R and Cyst Growth in Polycystic Kidney Disease. *Journal of the American Society of Nephrology*, 10.1681/ASN.0000000000000416 (2024).

40. Cabrita, I. *et al.* Cyst growth in ADPKD is prevented by pharmacological and genetic inhibition of TMEM16A in vivo. *Nature Communications* **11**, 4320 (2020).
41. Legue, E. & Liem, K.F., Jr. Tulp3 Is a Ciliary Trafficking Gene that Regulates Polycystic Kidney Disease. *Curr Biol* **29**, 803–812 e5 (2019).
42. Hwang, S.-h. *et al.* Kidney cystogenesis in embryonic- and adult-onset ADPKD is suppressed from lack of adenylyl cyclase targeting to cilia. *bioRxiv*, 2025.05.27.656198 (2025).
43. Walker, R.V. *et al.* Cilia-Localized Counterregulatory Signals as Drivers of Renal Cystogenesis. *Front Mol Biosci* **9**, 936070 (2022).
44. Ma, M., Gallagher, A.R. & Somlo, S. Ciliary Mechanisms of Cyst Formation in Polycystic Kidney Disease. *Cold Spring Harb Perspect Biol* **9**(2017).
45. Antignac, C. *et al.* The Future of Polycystic Kidney Disease Research--As Seen By the 12 Kaplan Awardees. *J Am Soc Nephrol* **26**, 2081–95 (2015).
46. Sun, Z. *et al.* A genetic screen in zebrafish identifies cilia genes as a principal cause of cystic kidney. *Development* **131**, 4085–93 (2004).
47. Caspary, T., Larkins, C.E. & Anderson, K.V. The graded response to Sonic Hedgehog depends on cilia architecture. *Dev Cell* **12**, 767–78 (2007).
48. Li, Y. *et al.* Deletion of ADP Ribosylation Factor-Like GTPase 13B Leads to Kidney Cysts. *J Am Soc Nephrol* **27**, 3628–3638 (2016).
49. Seixas, C. *et al.* Arl13b and the exocyst interact synergistically in ciliogenesis. *Mol Biol Cell* **27**, 308–20 (2016).
50. Gotthardt, K. *et al.* A G-protein activation cascade from Arl13B to Arl3 and implications for ciliary targeting of lipidated proteins. *Elife* **4**(2015).
51. Ivanova, A.A. *et al.* Biochemical characterization of purified mammalian ARL13B protein indicates that it is an atypical GTPase and ARL3 guanine nucleotide exchange factor (GEF). *J Biol Chem* **292**, 11091–11108 (2017).
52. Higginbotham, H. *et al.* Arl13b in primary cilia regulates the migration and placement of interneurons in the developing cerebral cortex. *Dev Cell* **23**, 925–38 (2012).
53. Mariani, L.E. *et al.* Arl13b regulates Shh signaling from both inside and outside the cilium. *Molecular Biology of the Cell* **27**, 3780–3790 (2016).
54. Gigante, E.D., Taylor, M.R., Ivanova, A.A., Kahn, R.A. & Caspary, T. ARL13B regulates Sonic hedgehog signaling from outside primary cilia. *eLife* **9**, e50434 (2020).
55. Van Sciver, R.E., Long, A.B., Katz, H.G., Gigante, E.D. & Caspary, T. Ciliary ARL13B inhibits developmental kidney cystogenesis in mouse. *Dev Biol* **500**, 1–9 (2023).
56. Suciu, S.K., Long, A.B. & Caspary, T. Smoothened and ARL13B are critical in mouse for superior cerebellar peduncle targeting. *Genetics* **218**(2021).
57. Cantagrel, V. *et al.* Mutations in the cilia gene ARL13B lead to the classical form of Joubert syndrome. *Am J Hum Genet* **83**, 170–9 (2008).
58. Humbert, M.C. *et al.* ARL13B, PDE6D, and CEP164 form a functional network for INPP5E ciliary targeting. *Proc Natl Acad Sci U S A* **109**, 19691–6 (2012).
59. Ferent, J. *et al.* The Ciliary Protein Arl13b Functions Outside of the Primary Cilium in Shh-Mediated Axon Guidance. *Cell Reports* **29**, 3356–3366.e3 (2019).
60. Piontek, K.B. *et al.* A functional floxed allele of Pkd1 that can be conditionally inactivated in vivo. *J Am Soc Nephrol* **15**, 3035–43 (2004).
61. Su, C.Y., Bay, S.N., Mariani, L.E., Hillman, M.J. & Caspary, T. Temporal deletion of Arl13b reveals that a mispatterned neural tube corrects cell fate over time. *Development* **139**, 4062–71 (2012).
62. Traykova-Brauch, M. *et al.* An efficient and versatile system for acute and chronic modulation of renal tubular function in transgenic mice. *Nat Med* **14**, 979–84 (2008).

63. Perl, A.K., Wert, S.E., Nagy, A., Lobe, C.G. & Whitsett, J.A. Early restriction of peripheral and proximal cell lineages during formation of the lung. *Proc Natl Acad Sci U S A* **99**, 10482–7 (2002).
64. Bankhead, P. *et al.* QuPath: Open source software for digital pathology image analysis. *Scientific Reports* **7**, 16878 (2017).
65. Wilson, L. *et al.* Chronic activation of AMP-activated protein kinase leads to early-onset polycystic kidney phenotype. *Clinical Science* **135**, 2393–2408 (2021).
66. Piontek, K., Menezes, L.F., Garcia-Gonzalez, M.A., Huso, D.L. & Germino, G.G. A critical developmental switch defines the kinetics of kidney cyst formation after loss of Pkd1. *Nat Med* **13**, 1490–5 (2007).
67. Aggarwal, S. *et al.* SOX9 switch links regeneration to fibrosis at the single-cell level in mammalian kidneys. *Science* **383**, eadd6371 (2024).
68. Seeger-Nukpezah, T., Geynisman, D.M., Nikonova, A.S., Benzing, T. & Golemis, E.A. The hallmarks of cancer: relevance to the pathogenesis of polycystic kidney disease. *Nat Rev Nephrol* **11**, 515–34 (2015).
69. Happé, H. *et al.* Toxic tubular injury in kidneys from Pkd1-deletion mice accelerates cystogenesis accompanied by dysregulated planar cell polarity and canonical Wnt signaling pathways. *Human Molecular Genetics* **18**, 2532–2542 (2009).
70. Pazour, G.J., San Agustin, J.T., Follit, J.A., Rosenbaum, J.L. & Witman, G.B. Polycystin-2 localizes to kidney cilia and the ciliary level is elevated in orpk mice with polycystic kidney disease. *Curr Biol* **12**, R378–80 (2002).
71. Hanaoka, K. *et al.* Co-assembly of polycystin-1 and -2 produces unique cation-permeable currents. *Nature* **408**, 990–4 (2000).
72. Nauli, S.M. *et al.* Polycystins 1 and 2 mediate mechanosensation in the primary cilium of kidney cells. *Nature Genetics* **33**, 129–137 (2003).
73. Liu, J. *et al.* Non-parallel recombination limits cre-loxP-based reporters as precise indicators of conditional genetic manipulation. *genesis* **51**, 436–442 (2013).
74. Vooijs, M., Jonkers, J. & Berns, A. A highly efficient ligand-regulated Cre recombinase mouse line shows that *LoxP* recombination is position dependent. *EMBO reports* **2**, 292–297 (2001).
75. Hwang, S.H. *et al.* Tulp3 Regulates Renal Cystogenesis by Trafficking of Cystoproteins to Cilia. *Curr Biol* **29**, 790–802 e5 (2019).
76. Silva, L.M. *et al.* Inhibition of Hedgehog signaling suppresses proliferation and microcyst formation of human Autosomal Dominant Polycystic Kidney Disease cells. *Sci Rep* **8**, 4985 (2018).
77. Hsieh, C.-L., Jerman, S.J. & Sun, Z. Non-cell-autonomous activation of hedgehog signaling contributes to disease progression in a mouse model of renal cystic ciliopathy. *Human Molecular Genetics* **31**, 4228–4240 (2022).
78. Tran, P.V. *et al.* Downregulating hedgehog signaling reduces renal cystogenic potential of mouse models. *J Am Soc Nephrol* **25**, 2201–12 (2014).
79. Ma, M., Legué, E., Tian, X., Somlo, S. & Liem, K.F.J. Cell-Autonomous Hedgehog Signaling Is Not Required for Cyst Formation in Autosomal Dominant Polycystic Kidney Disease. *Journal of the American Society of Nephrology* **30**, 2103–2111 (2019).
80. Gombart, S., Houghtaling, S., Ho, T.-H. & Beier, D.R. Inhibition of Hedgehog signaling does not mitigate polycystic kidney disease severity in a Pkd1 mutant mouse model. *Journal of Cell Science*, jcs.264133 (2025).
81. Somatilaka, B.N. *et al.* Ankmy2 Prevents Smoothened-Independent Hyperactivation of the Hedgehog Pathway via Cilia-Regulated Adenylyl Cyclase Signaling. *Developmental Cell* **54**, 710–726.e8 (2020).

82. Palicharla, V.R. *et al.* Interactions between TULP3 tubby domain and ARL13B amphipathic helix promote lipidated protein transport to cilia. *Molecular Biology of the Cell* **0**, mbc.E22–10–0473 (2023).
83. Mukhopadhyay, S. *et al.* The ciliary G-protein-coupled receptor Gpr161 negatively regulates the Sonic hedgehog pathway via cAMP signaling. *Cell* **152**, 210–23 (2013).
84. Mukhopadhyay, S. *et al.* TULP3 bridges the IFT-A complex and membrane phosphoinositides to promote trafficking of G protein-coupled receptors into primary cilia. *Genes Dev* **24**, 2180–93 (2010).
85. Badgandi, H.B., Hwang, S.-h., Shimada, I.S., Loriot, E. & Mukhopadhyay, S. Tubby family proteins are adapters for ciliary trafficking of integral membrane proteins. *The Journal of Cell Biology* **216**, 743–760 (2017).

Figure 1

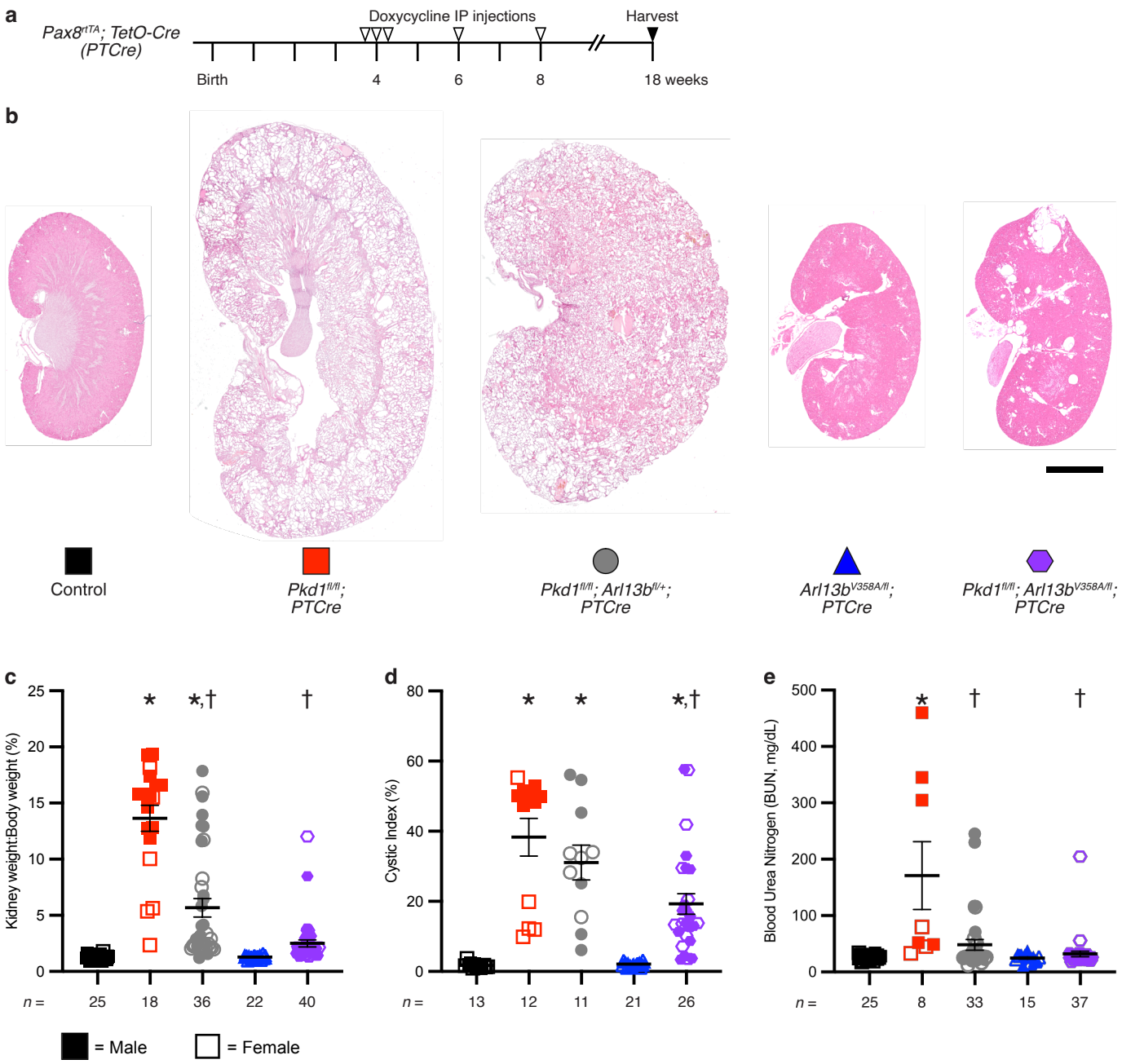
a
Pax8rtTA; TetO-Cre (PTCre)
Doxycycline IP injections
Harvest
Birth
4
6
8
18 weeks
b
Control
Pkd1fl/fl; PTCre
Pkd1fl/fl; Arl13bfl/+; PTCre
Arl13bV358A/fl; PTCre
Pkd1fl/fl; Arl13bV358A/fl; PTCre
c
Kidney weight:Body weight (%)
n = 25 18 36 22 40
d
Cystic Index (%)
n = 13 12 11 21 26
e
Blood Urea Nitrogen (BUN, mg/dL)
n = 25 8 33 15 37
= Male
= Female

Figure 2

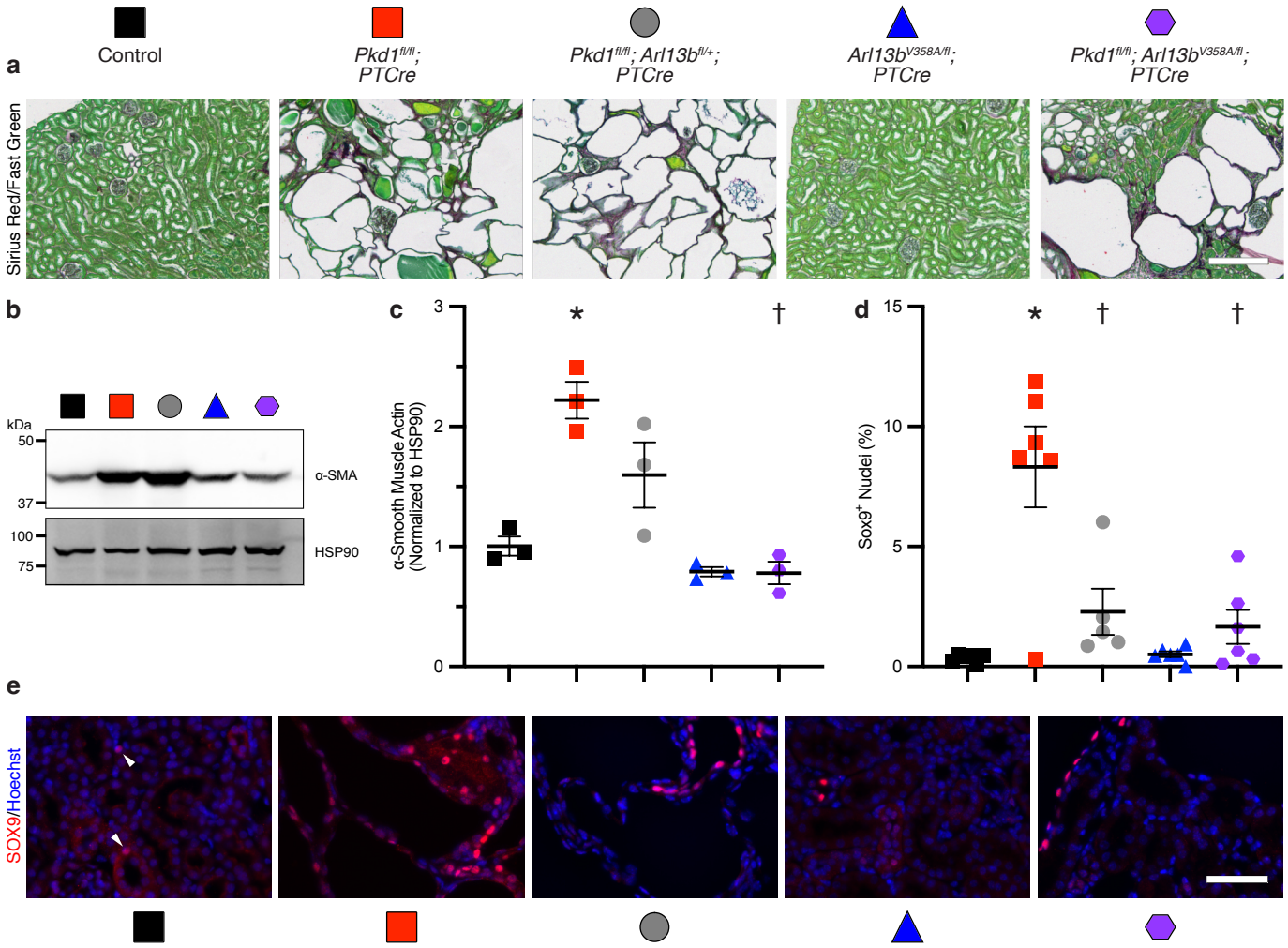
a
Control
Pkd1fl/fl; PTCre
Pkd1fl/fl; Arl13bfl/+; PTCre
Arl13bV358A/fl; PTCre
Pkd1fl/fl; Arl13bV358A/fl; PTCre
Sirius Red/Fast Green
b
kDa
50
37
100
75
α-SMA
HSP90
c
α-Smooth Muscle Actin (Normalized to HSP90)
3
2
1
0
*
†
d
Sox9+ Nuclei (%)
15
10
5
0
*
†
†
e
SOX9/Hoechst

Figure 3

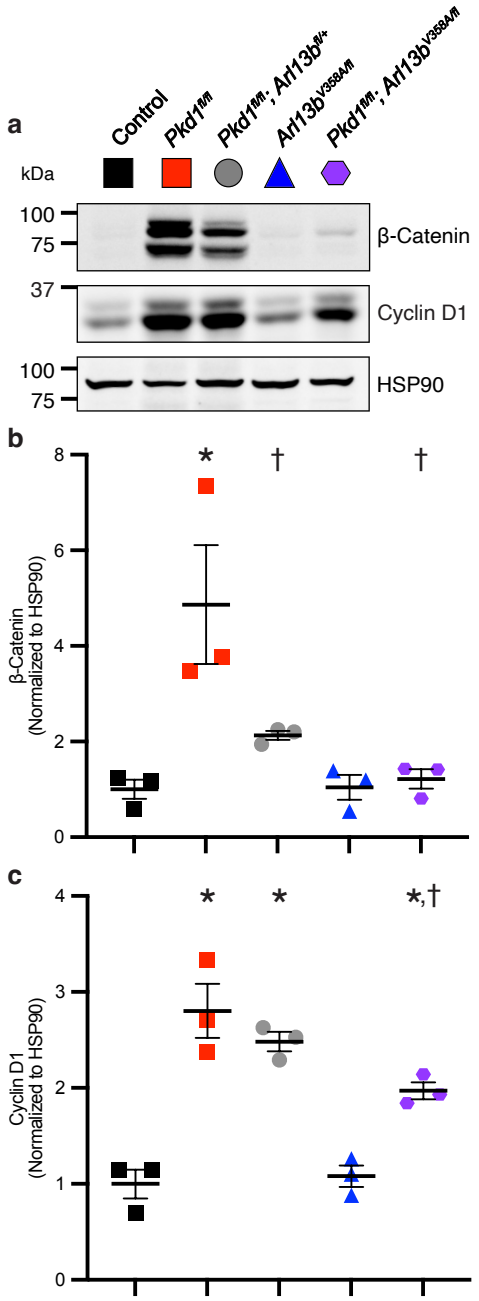
a
Control
Pkd1f/f
Pkd1f/f; Arl13bfl/+
Arl13bV358A/f
Pkd1f/f; Arl13bV358A/f
kDa
100
75
β-Catenin
37
Cyclin D1
100
75
HSP90
b
β-Catenin
(Normalized to HSP90)
8
6
4
2
0
*
†
†
c
Cyclin D1
(Normalized to HSP90)
4
3
2
1
0
*
*
*,†

Figure 4

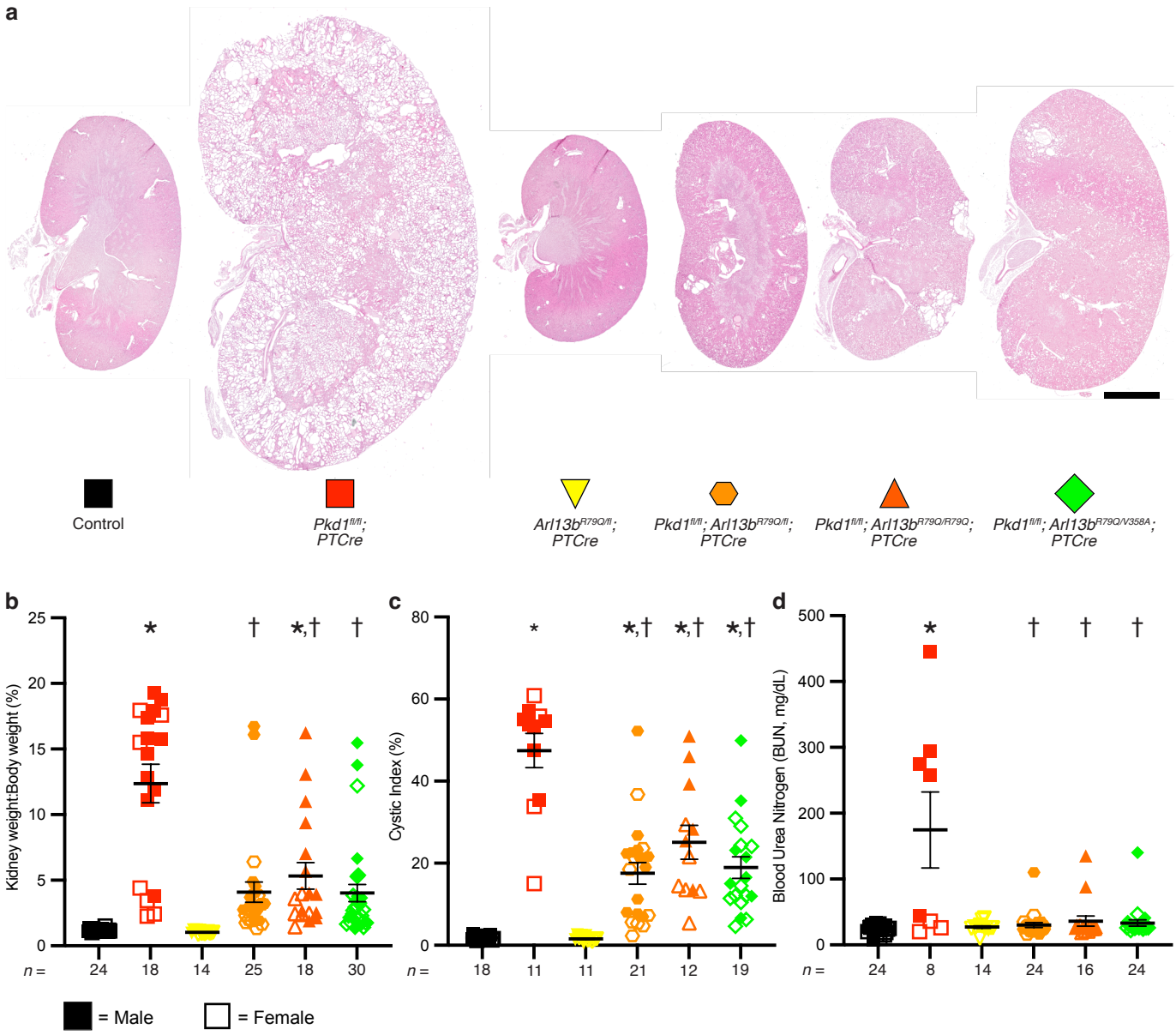
a
Control
Pkd1fl/fl; PTCre
Arl13bR79Q/fl; PTCre
Pkd1fl/fl; Arl13bR79Q/fl; PTCre
Pkd1fl/fl; Arl13bR79Q/R79Q; PTCre
Pkd1fl/fl; Arl13bR79Q/V358A; PTCre
b
Kidney weight:Body weight (%)
n = 24 18 14 25 18 30
c
Cystic Index (%)
n = 18 11 11 21 12 19
d
Blood Urea Nitrogen (BUN, mg/dL)
n = 24 8 14 24 16 24
= Male
= Female

Figure 5

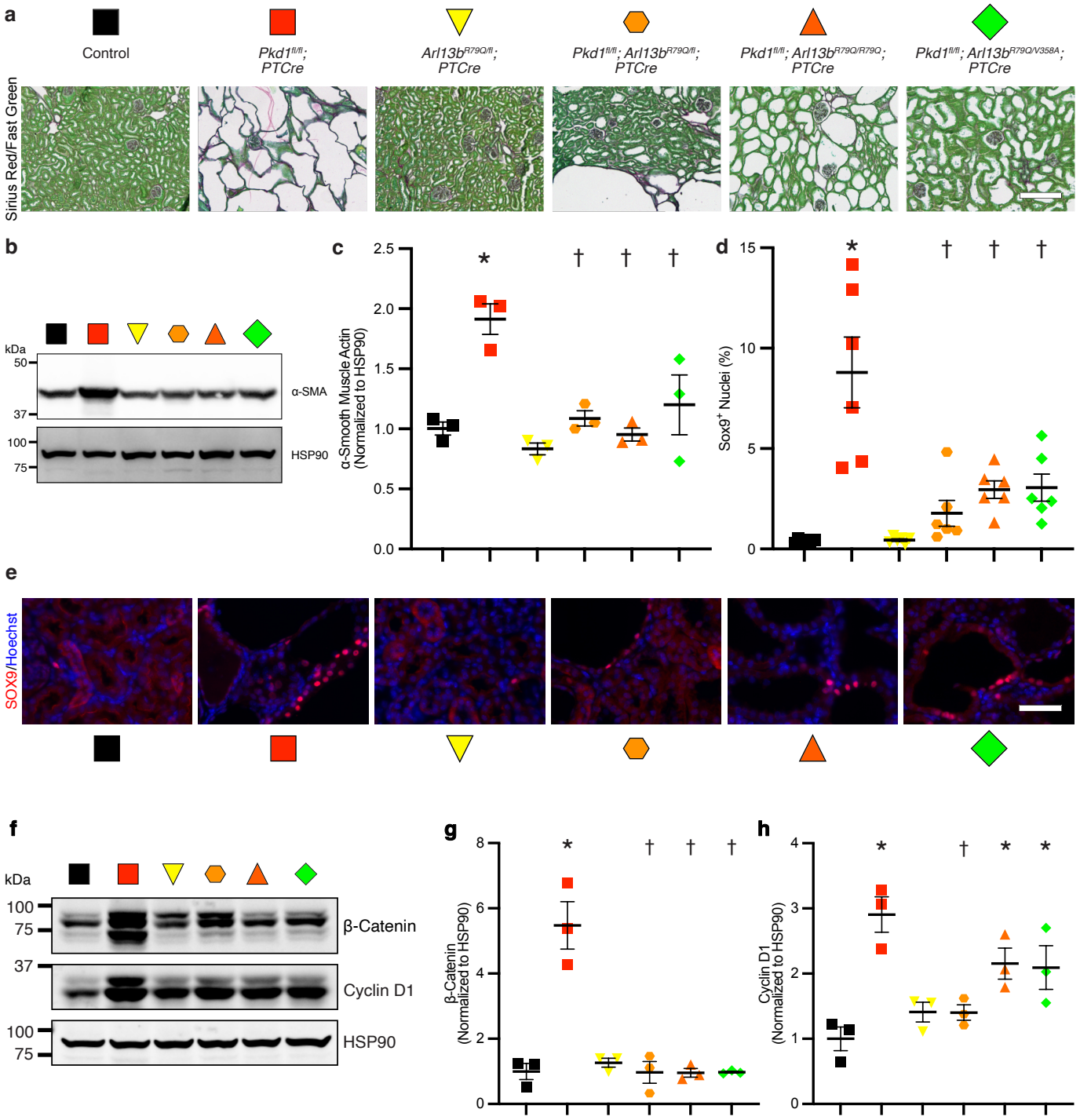
a
Control
Pkd1fl/fl; PTCre
Arl13bR79Q/fl; PTCre
Pkd1fl/fl; Arl13bR79Q/fl; PTCre
Pkd1fl/fl; Arl13bR79Q/R79Q; PTCre
Pkd1fl/fl; Arl13bR79Q/V358A; PTCre
Sirius Red/Fast Green
b
kDa
50
37
100
75
α-SMA
HSP90
c
α-Smooth Muscle Actin (Normalized to HSP90)
2.5
2.0
1.5
1.0
0.5
0.0
d
Sox9+ Nuclei (%)
15
10
5
0
e
SOX9/Hoechst
f
kDa
100
75
37
β-Catenin
Cyclin D1
HSP90
g
β-Catenin (Normalized to HSP90)
8
6
4
2
0
h
Cyclin D1 (Normalized to HSP90)
4
3
2
1
0

Figure 6

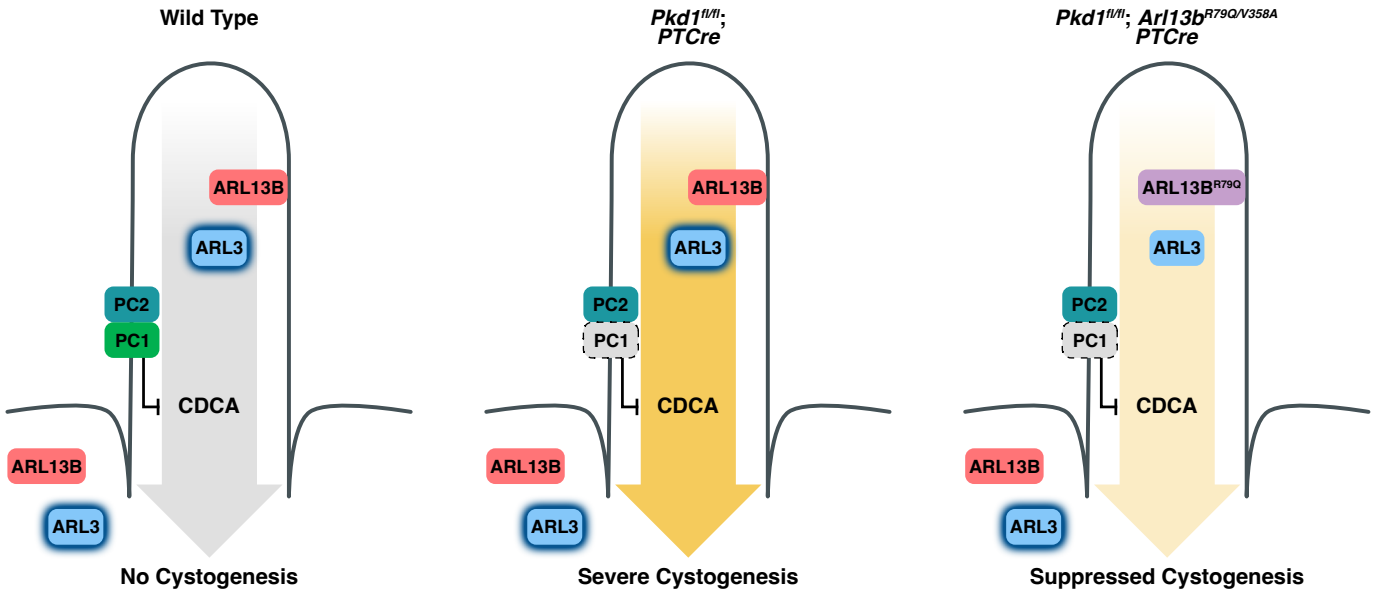
Wild Type
ARL13B
ARL3
PC2
PC1
CDCA
ARL13B
ARL3
No Cystogenesis
Pkd1fl/fl; PTCre
ARL13B
ARL3
PC2
PC1
CDCA
ARL13B
ARL3
Severe Cystogenesis
Pkd1fl/fl; Arl13bR79Q/V358A PTCre
ARL13BR79Q
ARL3
PC2
PC1
CDCA
ARL13B
ARL3
Suppressed Cystogenesis